

This is the peer reviewed version of the following article:

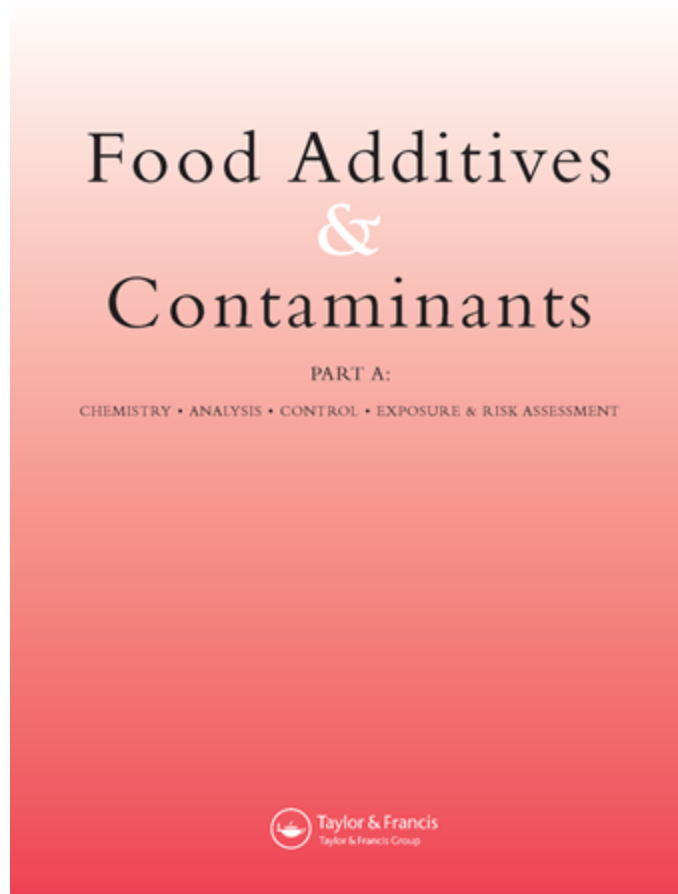
Multivariate image analysis for the rapid detection of residues from packaging remnants in former foodstuff products (FFPs)-a feasibility study / Calvini, R.; Luciano, A.; Ottoboni, M.; Ulrici, A.; Tretola, M.; Pinotti, L.. - In: FOOD ADDITIVES & CONTAMINANTS. PART A. CHEMISTRY, ANALYSIS, CONTROL, EXPOSURE & RISK ASSESSMENT. - ISSN 1944-0049. - 37:8(2020), pp. 1399-1411. [10.1080/19440049.2020.1769195]

*Terms of use:*

The terms and conditions for the reuse of this version of the manuscript are specified in the publishing policy. For all terms of use and more information see the publisher's website.

19/04/2024 21:58

(Article begins on next page)



**Multivariate image analysis for the rapid detection of residues from packaging remnants in former foodstuff products (FFPs) – a feasibility study**

Journal:	<i>Food Additives and Contaminants</i>
Manuscript ID	TFAC-2019-499.R1
Manuscript Type:	Original Article
Date Submitted by the Author:	n/a
Complete List of Authors:	Calvini, Rosalba; University of Modena and Reggio Emilia, Department of Life Sciences and Interdepartmental Centre BIOGEST-SITEIA Luciano, Alice; University of Milan, Department of Health, Animal Science and Food Safety (VESPA) Ottoboni, Matteo; University of Milan, Department of Health, Animal Science and Food Safety (VESPA) Ulrici, Alessandro; University of Modena and Reggio Emilia, Department of Life Sciences and Interdepartmental Centre BIOGEST-SITEIA Tretola, Marco; University of Milan, Department of Health, Animal Science and Food Safety (VESPA); Agroscope, Institute for Livestock Sciences

	Pinotti, Luciano; University of Milan, Department of Health, Animal Science and Food Safety (VESPA)
Methods/Techniques:	Screening assays, Chemometrics
Additives/Contaminants:	Packaging
Food Types:	Animal feedingstuffs, Animal feed
Abstract:	<p>From a circular economy perspective, feeding livestock with food leftovers or former foodstuff products (FFPs) could be an effective option aimed at exploiting food leftover resources and reducing food losses. FFPs are valuable energy sources, characterized by a beneficial starch/sugar content, and also fats. However, besides these nutritional aspects, safety is a key concern given that FFPs are generally derived from packaged food. Packaging materials, such as plastics and paper, are not accepted as a feed ingredient which means that residues should be rigorously avoided. A sensitive and objective detection method is thus essential for an accurate risk evaluation throughout the former food production chain. To this end, former food samples were collected in processing plants of two different European countries and subjected to multivariate analysis of red, green, and blue (RGB) microscopic images, in order to evaluate the possible application of this nondestructive technique for the rapid detection of residual particles from packaging materials. Multivariate Image Analysis (MIA) was performed on single images at the pixel level, which essentially consisted in an exploratory analysis of the image data by means of Principal Component Analysis, which highlighted the differences between packaging and foodstuff particles, based on their colour. The whole dataset of images was then analysed by means of a multivariate data dimensionality reduction method known as the colourgrams approach, which identified clusters of images sharing similar features and also highlighted outlier images due to the presence of packaging particles. The results obtained in this feasibility study demonstrated that MIA is a promising tool for a rapid automated method for detecting particles of packaging materials in FFPs.</p>

SCHOLARONE™  
Manuscripts

1  
2  
3 1 **Multivariate image analysis for the rapid detection of residues from packaging**  
4  
5  
6 2 **remnants in former foodstuff products (FFPs) – a feasibility study**  
7  
8

9 3 Rosalba Calvini<sup>1</sup>, Alice Luciano<sup>2</sup>, Matteo Ottoboni<sup>2</sup>, Alessandro Ulrici<sup>\*1</sup>, Marco  
10 4 Tretola<sup>2,§</sup>, Luciano Pinotti<sup>2</sup>  
11  
12  
13  
14  
15 5

16  
17 6 <sup>1</sup> *Department of Life Sciences and Interdepartmental Centre BIOGEST-SITEIA, University of*  
18  
19 7 *Modena and Reggio Emilia, Pad. Besta, Via Amendola, 2, Reggio Emilia, 42122, Italy*

20  
21 8 <sup>2</sup> *Department of Health, Animal Science and Food Safety, VESPA, University of Milan, Milano,*  
22  
23  
24 9 *Italy*

25  
26 10 <sup>§</sup>*Present address: Agroscope, Institute for Livestock Sciences, Posieux, Switzerland;*

27  
28 11 *\* Corresponding author: Prof. Alessandro Ulrici*

29  
30 12 *Department of Life Sciences and Interdepartmental Centre BIOGEST-SITEIA, University of*  
31  
32  
33 13 *Modena and Reggio Emilia, Pad. Besta, Via Amendola, 2, Reggio Emilia, 42122, Italy*

34  
35 14 *e-mail: [alessandro.ulrici@unimore.it](mailto:alessandro.ulrici@unimore.it)*  
36  
37  
38 15  
39  
40  
41  
42  
43  
44  
45  
46  
47  
48  
49  
50  
51  
52  
53  
54  
55  
56  
57  
58  
59  
60

1  
2  
3 16 **Multivariate image analysis for the rapid detection of residues from packaging**  
4  
5  
6 17 **remnants in former foodstuff products (FFPs) – a feasibility study**  
7  
8

9 18 **Abstract**  
10

11 19 From a circular economy perspective, feeding livestock with food leftovers or former foodstuff  
12 20 products (FFPs) could be an effective option aimed at exploiting food leftover resources and reducing  
13 21 food losses. FFPs are valuable energy sources, characterized by a beneficial starch/sugar content, and  
14 22 also fats. However, besides these nutritional aspects, safety is a key concern given that FFPs are  
15 23 generally derived from packaged food. Packaging materials, such as plastics and paper, are not  
16 24 accepted as a feed ingredient which means that residues should be rigorously avoided. A sensitive  
17 25 and objective detection method is thus essential for an accurate risk evaluation throughout the former  
18 26 food production chain. To this end, former food samples were collected in processing plants of two  
19 27 different European countries and subjected to multivariate analysis of red, green, and blue (RGB)  
20 28 microscopic images, in order to evaluate the possible application of this nondestructive technique for  
21 29 the rapid detection of residual particles from packaging materials. Multivariate Image Analysis (MIA)  
22 30 was performed on single images at the pixel level, which essentially consisted in an exploratory  
23 31 analysis of the image data by means of Principal Component Analysis, which highlighted the  
24 32 differences between packaging and foodstuff particles, based on their colour. The whole dataset of  
25 33 images was then analysed by means of a multivariate data dimensionality reduction method known  
26 34 as the colourgrams approach, which identified clusters of images sharing similar features and also  
27 35 highlighted outlier images due to the presence of packaging particles. The results obtained in this  
28 36 feasibility study demonstrated that MIA is a promising tool for a rapid automated method for  
29 37 detecting particles of packaging materials in FFPs.  
30  
31  
32  
33  
34  
35  
36  
37  
38

1  
2  
3  
4  
5  
6  
7  
8  
9  
10  
11  
12  
13  
14  
15  
16  
17  
18  
19  
20  
21  
22  
23  
24  
25  
26  
27  
28  
29  
30  
31  
32  
33  
34  
35  
36  
37  
38  
39  
40  
41  
42  
43  
44  
45  
46  
47  
48  
49  
50  
51  
52  
53  
54  
55  
56  
57  
58  
59  
60

39 **Keywords**

40 Former foodstuffs; packaging remnants; colourgrams; Multivariate Image Analysis (MIA); feed; food  
41 safety.

For Peer Review Only

## 1. Introduction

The livestock sector is inevitably going to involve trade-offs between feed security, feed safety, animal welfare, environmental sustainability and economic development. A common denominator among many of these issues, which are often politically-sensitive, is sustainability. In fact, converting losses from the food industry into ingredients for the feed industry, thereby keeping food losses in the food chain, can be considered a positive cycle that should be implemented worldwide.

Food leftovers or Former Foodstuffs Products (FFPs) are animal feed ingredients consisting of processed and ready-to-eat food products, no longer suitable for human consumption due to logistical, manufacturing or packaging defects. Former food products mainly consist of leftovers from the baking industry (e.g. bread, pasta) and confectionery products (e.g. chocolates, biscuits). Rejected bread, various biscuit products, high-quality baked goods and confectionary from industrial biscuit bakeries are dried and consecutively sorted, unpacked, ground and sieved to create suitable ingredients, which replace some of the existing raw materials in various animal compound feed (Pinotti et al. 2019; Ottoboni et al. 2019; Tretola et al. 2019a, 2019b). Based on the nutritional facts reported for humans, FFPs are extremely rich in carbohydrates, and depending on their origin, also in fats (Giromini et al. 2017). All these factors make FFPs particularly suited to the circular economy: FFPs represent a way by which convert losses from the food industry into ingredients for the feed industry (Pinotti et al. 2019).

Although FFPs are nutritious and safe from a microbiological point of view (Tretola et al. 2017a, 2017b), they may generate other safety issues, such as those related to the presence of packaging remnants. FFPs are un-packaged automatically in order to process a large amount of product. Feed processors routinely remove the packaging from FFPs mechanically in the feed plant; however, despite the removal of most of the packaging, small amounts of wrapping materials remain in the resulting feed. Consequently, a small amount of packaging remnants in the final product (feed) appears to be unavoidable (Tretola et al. 2017a, 2017b).

1  
2  
3 67 Typical remnant residues in FFPs include paper/paperboard, aluminum foil, and plastics, all of  
4  
5 68 which can remain as residues in the final product. In Tretola et al. (2019a) paperboard was the most  
6  
7  
8 69 detected contaminant followed by aluminum foil, and then plastic. Among these, plastics are  
9  
10 70 becoming extremely important especially when small particles are considered. Microplastics are  
11  
12 71 usually defined as plastic particles with a size smaller than 5 mm for their largest dimension. In  
13  
14 72 general, particles with a size equal to 1–2 mm or larger can be visually detected, manually extracted  
15  
16 73 and quantified based on weight. This procedure has become a daily practice in the monitoring of  
17  
18 74 former foodstuffs for use in animal feeds (Van Raamsdonk et al. 2020).

19 75 However, irrespective of material type, packaging remnants are generally not accepted as a feed  
20  
21 76 ingredient by several authorities, which prohibit the sale of feedstuffs containing packaging materials  
22  
23 77 from the agri-food industry. By contrast, some national authorities have indicated that a minimum  
24  
25 78 percentage of packaging remnants in FFPs is unavoidable and not risky either for animals or humans  
26  
27 79 (Van Raamsdonk et al. 2011; Van Raamsdonk et al. 2012). From a safety point of view, in most  
28  
29 80 analysed samples, the presence of these foreign materials is negligible and below the maximum limit  
30  
31 81 established by some control authorities/bodies (e.g. 0.12% w/w set by the German Federal Ministry  
32  
33 82 of Food, Agriculture and Consumer Protection) (Pinotti et al. 2019; Tretola et al. 2017a; Tretola et al.  
34  
35 83 2019a).

36  
37 84 In terms of particles dimension, it has been established that remnants normally present in FFPs are  
38  
39 85 mainly in the > 800 µm mesh fraction (Tretola et al., 2017a; van Raamsdonk et al., 2012).  
40  
41 86 Quantification of particles smaller than 400 µm is generally too laborious and, according to van  
42  
43 87 Raamsdonk et al. (2012), these smaller particles are excluded from the quantification, since their  
44  
45 88 share in the total weight is insignificant.

46  
47 89 A sensitive and objective detection method is therefore essential for tracing and quantifying  
48  
49 90 packaging remnants in FFPs.

50  
51 91 The detection and quantification of packaging remnants in bakery products using a  
52  
53 92 stereomicroscope was proposed by the RIKILT Institute (Wageningen) (Van Raamsdonk et al. 2011;



1

2

3 93 Van Raamsdonk et al. 2012). Amato et al. (2017) used a similar approach to develop a sensitive

4 94 gravimetric method, for routine official controls for the determination of packaging residues in feed.

7 95 The two proposed methods can be summarised as follows: (1) visual selection of the undesired

9 96 ingredients i.e. remnants of packaging materials; (2) weighing of the selected materials; (3) defatting;

11 97 (4) dehydration; (5) final weighing; and (6) reporting of weight and percentage. In both cases however

13 98 the methods appear complex, time consuming and analyst sensitive.

16 99 In this respect, some of the authors of the present work (Tretola et al. 2017b) used computer sensing

18 100 to visualize packaging remnants. The results showed that computer vision, when coupled with a

20 101 stereomicroscope for image acquisition, acts a rapid qualitative screening approach to estimate the

22 102 presence of foreign materials in food and feed, with little laborious and subjective human visual

24 103 involvement (Tretola et al. 2017b). Tretola et al. (2019a) also investigated the use of an electronic

26 104 nose (e-Nose) to detect these contaminants in FFPs. The results indicated that an e-Nose can be used

28 105 for rapidly screening for the presence of **presumed packaging remnants of aluminum, plastics and**

30 106 **paperboard** in FFPs, when the food/feed matrix is characterized by low variability (e.g. same

32 107 producer, same odor print).

34 108 The aim of this work was to assess the potential of Multivariate Image Analysis (MIA) to

36 109 automatically detect packaging residues **using red, green, and blue (RGB) images** of FFP samples

38 110 acquired with a stereomicroscope. **The most common statistical tool applied in MIA is Principal**

40 111 **Component Analysis (PCA), which highlights similarities and differences among groups of pixels**

42 112 **based on their spectral features (i.e., on their colour for RGB images) (Esbensen et al. 2011; Prats-**

44 113 **Montalbán et al. 2011; Geladi et al. 1989).**

46 114 **In practical applications for quality monitoring, a high number of images need to be acquired in order**

48 115 **to calculate robust and reliable models. In this case, it is necessary to consider both within-image and**

50 116 **between-images variability, to properly characterize each single sample and to account at the same**

52 117 **time for the variations between the different samples (Gowen et al. 2011; Duchesne et al. 2016;**

54 118 **Dorrepaal et al. 2016). Therefore, in order to overcome data handling issues, an image-level approach**

1  
2  
3 119 is fundamental, which is based on extracting from each image a feature vector summarizing the  
4  
5 120 information needed for the analysis (Ferrari et al. 2013; Calvini et al. 2016).

7  
8 121 The colourgrams method follows this image-level approach and is specifically implemented for the  
9  
10 122 analysis of RGB images (Antonelli et al. 2004). It converts each RGB image of the dataset into a one-  
11  
12 123 dimensional signal, the colourgram, which summarizes the colour features of the corresponding  
13  
14 124 image. The colourgrams are then collected into a data matrix in which each row corresponds to the  
15  
16  
17 125 signal derived from a specific image of the dataset. The colourgrams matrix can then be analysed  
18  
19 126 using common multivariate statistical methods, e.g. PCA, in order to gain an exploratory overview  
20  
21 127 of the whole dataset of images, to identify clusters of images sharing similar features, and to highlight  
22  
23  
24 128 possible outliers.

25  
26 129 The colourgrams approach has been successfully applied in several case studies above all related to  
27  
28 130 the analysis of food matrices by means of RGB imaging (Ulrici et al. 2012; Orlandi et al. 2018a;  
29  
30 Orlandi et al. 2018b; Girauda et al. 2018).

31 131  
32  
33 132 In the present study, the images of FFP samples were analysed using both the pixel-level and the  
34  
35 133 image-level approaches, in order evaluate their effectiveness in detecting the presence of possible  
36  
37  
38 134 particles derived from packaging residues.

## 41 42 136 2. Materials and methods

### 43 44 45 137 2.1 FFPs samples and image acquisition

46  
47  
48 138 Six different commercial samples of FFPs, originating from two European countries, were used  
49  
50 139 (Table 1). Three samples (FFPs A, B and D) were obtained from an FFP processing plant in Country  
51  
52 140 1, while 3 samples (FFPs C, E, F) were from an FFP processor in Country 2.

53  
54  
55 141 All samples were produced from different food materials, including bakery products, broken biscuits  
56  
57  
58 142 and chocolates, confectionery products (e.g. croissants, chocolate), surplus bread, rice cakes, salty  
59  
60 143 snacks, and breakfast cereals. For all the FFP samples, a randomly selected aliquot of 5g was placed

1  
2  
3 144 in a large Petri dish (PS Ø 90, Colaver, Milan) in a manner to form a single layer. The amount of  
4  
5 145 former food aliquots to be analysed was chosen based on a previous study, which verified  
6  
7  
8 146 homogenous distribution of packaging remnants in reduced amount of former food samples (Tretola  
9  
10 147 et al., 2017a). Specifically, correspondence between packaging remnants levels found in 100 g of an  
11  
12 148 FFP sample and relative sub-samples of 2 g was verified by Tretola and coworkers (2017a). In order  
13  
14  
15 149 to increase sampling representativeness, in this study sample quantity was increased to 5g.

16  
17  
18 150 Using a stereo microscope (OLYMPUS SZX9), each sample was investigated separately, taking  
19  
20 151 utmost care in order to avoid any contamination in line with laboratory Standard Operating  
21  
22 152 Procedures (SOPs) for remnants of packaging materials. For each sample, from 5 to 13 images, with  
23  
24  
25 153 or without packaging remnants, were acquired using a digital camera (CoolSNAP-Pro cf Color or  
26  
27 154 AxioCam MRc coupled with a 0.63 port) equipped with an image analysis software (Image-Pro Plus  
28  
29 155 7.0; Media Cybernetics Inc., Rockville, MD, USA). The pixel size of the acquired RGB images was  
30  
31 156 equal to  $1392 \times 1040$ , corresponding to a surface area of  $2.8 \times 2.1$  mm. Therefore, the size of a single  
32  
33  
34 157 pixel was equal to  $2 \times 2 \mu\text{m}$ , which is much smaller than the minimum size of  $400 \mu\text{m}$ , as reported  
35  
36 158 by van Raamsdonk et al. (2012).

## 39 159 40 41 160 **2.2 Image analysis**

42  
43  
44 161 In order to highlight the potential of MIA to gain a preliminary evaluation at the pixel level of the  
45  
46 162 colour differences between FFP matrices and particles of foreign materials derived from packaging,  
47  
48  
49 163 one image of sample A containing a plastic piece was analysed by means of PCA.

50  
51 164 The key aspect of PCA consists in representing a multivariate dataset with a low number of orthogonal  
52  
53 165 variables, named principal components (PCs), which are linear combinations of the original variables  
54  
55 166 (Prats-Montalbán et al. 2011; Geladi et al. 1989). The principal components are calculated so that the  
56  
57  
58 167 first PC (PC1) describes the direction of maximum variance in the data, the second PC (PC2) is  
59  
60 168 orthogonal to PC1 and accounts for the maximum residual variance (i.e. the variance not described

1  
2  
3 169 by PC1), and the same applies for the subsequent PCs. In order to apply PCA to RGB images, the  
4  
5 170 three-dimensional data array composed of  $m$  pixel rows,  $n$  pixel columns and the three RGB channels,  
6  
7  
8 171 is unfolded into a bidimensional data matrix with  $m \times n$  rows, corresponding to the number of pixels  
9  
10 172 in the image, and three columns corresponding to the RGB values.

11  
12 173 The PCA decomposition of the unfolded RGB image ( $X$ ) can be expressed as follows:

$$14 \quad \mathbf{X} = \mathbf{TP}^T + \mathbf{E} \quad (1)$$

15 174  
16  
17 175 where  $T$  is the score matrix containing the pixel coordinates in the PCs space,  $P$  is the loading matrix  
18  
19 176 describing the relevance of the original variables (i.e. the R, G and B channels) in defining the PCs,  
20  
21  
22 177 and  $E$  denotes the residual matrix accounting for residual variation not included in the model.

23  
24 178 In order to recover the spatial structure of the image, the score vector of each PC can be refolded into  
25  
26 179 a score image with the same spatial dimensions as the original RGB image.

27  
28 180 The same approach described for RGB images can also be applied to more complicated images, such  
29  
30  
31 181 as multispectral or hyperspectral images, which have more than three channels.

32  
33 182 In this study, PCA was applied both to the RGB image “as is” as well as to the augmented RGB image  
34  
35 183 that was obtained by considering additional colour-related channels derived from the RGB values.

36  
37 184 These additional colour parameters include lightness ( $L$ ), the relative colours (relative Red, relative  
38  
39  
40 185 Green and relative Blue), and hue ( $H$ ), saturation ( $S$ ), and intensity ( $I$ ) obtained by converting the  
41  
42 186 RGB colour space into the HSI colour space.

43  
44 187 Table 2 gives the complete list of the colour-related parameters, together with the corresponding  
45  
46  
47 188 equations.

48  
49 189 While in RGB images each pixel is characterized by the three R, G and B channels, in the augmented  
50  
51 190 RGB image, each pixel is defined by seven parameters in addition to the RGB values, for a total of  
52  
53  
54 191 10 channels. For both images, PCA was applied considering autoscaling as the data preprocessing  
55  
56 192 method.

57  
58 193 The whole dataset of 43 images was then analysed at the image-level by converting each image into  
59  
60 194 the corresponding colourgram. The first step in this conversion consists in the same unfolding

1  
2  
3 195 procedure described for the pixel-level analysis. The unfolded RGB matrix is then expanded by  
4  
5 196 adding further columns containing additional colour-related parameters. These parameters include  
6  
7  
8 197 the quantities reported in Table 2 and the score vectors obtained by analysing the RGB data matrix  
9  
10 198 by means of PCA and considering three preprocessing methods (i.e., no preprocessing, mean  
11  
12 199 centering and autoscaling). For all the variables, the corresponding frequency distribution curves are  
13  
14  
15 200 calculated, considering the entire range of variability of each single variable and dividing it into 256  
16  
17 201 bins. Then, for each image the corresponding colourgram is calculated by merging in sequence the  
18  
19 202 frequency distribution curves of the considered colour-related parameters and by adding, at the end  
20  
21  
22 203 of the signal, the loading vectors of the PCA models, thereby obtaining a 4900-point long signal.  
23  
24 204 Further details about the algorithm used to calculate the colourgrams can be found in (Antonelli et al.  
25  
26 205 2004).

27  
28 206 The resulting matrix of colourgrams was then analysed by means of PCA using autoscaling as a signal  
29  
30  
31 207 preprocessing method. The exploratory analysis of the dataset at the image-level helped to identify  
32  
33 208 the colour-related features characterizing images of FFP samples with packaging residuals.

34  
35 209 The RGB images were converted into the corresponding colourgrams using Colourgrams GUI  
36  
37  
38 210 (Calvini et al., 2020), a user-friendly interface running under MATLAB (The Mathworks, USA).  
39  
40 211 Colourgrams GUI is freely downloadable from <http://www.chimslab.unimore.it/downloads/>. The  
41  
42 212 PCA models were calculated using PLS\_Toolbox (ver. 8.5, Eigenvector Research Inc., USA) and  
43  
44 213 MIA Toolbox (ver. 3.0.4, Eigenvector Research Inc., USA).

46  
47 214

### 49 215 **3. Results**

#### 51 216 **3.1 Pixel-level analysis**

52  
53  
54 217 To illustrate the potential of MIA performed at the pixel-level, the image reported in Figure 1 was  
55  
56 218 analysed by means of PCA. This image represents a former food matrix contaminated with a semi-  
57  
58 219 opaque plastic residue. Figure 1 also shows the corresponding red, green and blue channels, reported  
59  
60  
220 separately from each other as gray-scale images.

1  
2  
3 221 The PCA model was calculated considering 2 PCs, accounting for 99.76% of the total variance. In  
4  
5 222 the corresponding PC1-PC2 score plot reported in Figure 2.A, each object represents one pixel of the  
6  
7  
8 223 RGB image. In this plot, the objects are coloured according to the score density, i.e. a yellowish  
9  
10 224 colour corresponds to an area of the PC1-PC2 score space with a high density of pixels, while blue  
11  
12 225 indicates an area with a low density of pixels. There are two main clusters of pixels in the figure. A  
13  
14 226 comparison of the PC1-PC2 score plot with the corresponding score images reported in Figure 2.C-  
15  
16  
17 227 D reveals that the pixels with positive score values for both PC1 and PC2 are mainly ascribable to the  
18  
19 228 piece of plastic. A compact way to simultaneously evaluate the information provided by both PC1  
20  
21 229 and PC2 is reported in Figure 2.E, which shows the composite false-colour image obtained by  
22  
23  
24 230 superimposing the PC1 and PC2 score images using the red and green channels, respectively.  
25  
26 231 The PC1 and PC2 loading vectors, reported in Figure 2.B, show which channels contribute most to  
27  
28 232 the separation. The three R, G, and B channels have similar positive loading values on PC1, indicating  
29  
30 233 that the three channels have a comparable contribution in the definition of PC1. Thus, PC1 essentially  
31  
32 234 describes variations of lightness in the image. Conversely, in the PC2 loading vector, the R and B  
33  
34 235 channels have a high influence on the model, while the G channel has a loading value close to zero.  
35  
36  
37 236 In addition, the R channel has a negative contribution on PC2, while the B channel has a positive  
38  
39 237 contribution on PC2. Therefore, compared to the pixels of the FFP matrix, the pixels of the piece of  
40  
41 238 plastic generally have higher values in the blue channel and lower values in the red channel, while  
42  
43 239 the green channel does not seem to contribute much to separating the two components of the image.  
44  
45  
46 240 In summary, the fact that the plastic residue has high positive scores for both PC1 and PC2, can be  
47  
48 241 ascribed to its brighter and more bluish colour with respect to the FFP.  
49  
50  
51 242 To better highlight the colour-related differences between the former food and the plastic residue in  
52  
53 243 this image, we also used PCA on the augmented RGB image. The optimal dimensionality of the PCA  
54  
55 244 model was 3 PCs and accounted for 98.92% of the total variance. In the PC1-PC3 score space reported  
56  
57 245 in Figure 3.A, the pixels of the image are grouped into two main clusters. The pixel cluster lying at  
58  
59 246 positive values of both the PC1 and PC3 score vectors is due to the pixels of the plastic particle. In

1  
2  
3 247 fact, the score images of PC1 and PC3 (Figure 3.C and Figure 3.D, respectively) highlight that the  
4  
5 248 pixels of the plastic residue generally have higher scores than the pixels of the FFP. Figure 3.E reports  
6  
7  
8 249 the composite false-colour image of the PC1 and PC3 scores, further confirming the differences  
9  
10 250 between the former food and the plastic residue.  
11  
12 251 Since the pixels of the plastic particle have high score values for both PC1 and PC3, the colour-related  
13  
14 252 variables that are the most relevant for detecting the plastic fragment are those with loading  
15  
16  
17 253 coefficients of the same sign (i.e. positive or negative) on both PC1 and PC3. For example, relative  
18  
19 254 blue (rB) has positive loading coefficients for both PC1 and PC3, therefore the pixels of the plastic  
20  
21  
22 255 piece have higher rB values than those of the former food matrix. Conversely, saturation (S) and  
23  
24 256 relative red (rR) have negative loading coefficients on PC1 and PC3, suggesting that the pixels of the  
25  
26 257 plastic residue have lower S and rR values than those of the FFP.  
27  
28 258 In order to confirm the results obtained by PCA, Figure 4.A and Figure 4.B show the gray-scale  
29  
30  
31 259 images of the rB and S parameters, respectively. The plastic residue has generally higher rB values  
32  
33 260 and lower saturation values than the food matrix, as previously found by PCA. The presence of the  
34  
35 261 plastic piece is also much more evident in the rB and S gray-scale images than the images of the  
36  
37  
38 262 single RGB channels reported in Figure 1. This suggests that considering additional colour-related  
39  
40 263 parameters better highlights the image features that are not clearly distinguishable from just the R, G  
41  
42 264 and B values.  
43  
44 265 The histograms of rB and S are reported in Figure 4.C and Figure 4.D, respectively. In both cases,  
45  
46  
47 266 the histograms have a bimodal distribution due to the fact that the plastic fragment and the former  
48  
49 267 food matrix have different rB and S values.  
50  
51 268 In order to verify whether the two peaks in the rB histogram were due above all to the differences  
52  
53  
54 269 between plastic and FFP, a reconstructed image was obtained by visualizing in the original RGB  
55  
56 270 domain only the pixels with rB values higher than 0.24 (i.e., the pixels whose rB values fall in the  
57  
58 271 blue area highlighted in Figure 4.C), while the remaining pixels are represented in black. As shown  
59  
60 272 in Figure 4.E, the majority of the selected pixels belong to the plastic residual. The same procedure

1  
2  
3 273 was also carried out for the saturation parameter, and in this case only the pixels with S values lower  
4  
5 274 than 0.45 (gray area in Figure 4.D) are reconstructed in Figure 4.F.

7  
8 275

### 10 276 **3.2 Image-level analysis**

11  
12 277 Concerning the image-level analysis of the whole image dataset, PCA was applied to the colourgram  
13  
14 278 matrix considering 3 PCs, which account for 68.67% of the total variability. In the PC1-PC2 score  
15  
16  
17 279 plot reported in Figure 5.A, each object represents the colourgram of one image, and the objects are  
18  
19 280 coloured according to the corresponding former food sample, while the marker indicates the presence  
20  
21 281 and nature of the packaging residues. For a better interpretation of the results, the labels in the score  
22  
23  
24 282 plot indicate the names of the corresponding images, and the most relevant sample images are also  
25  
26 283 reported.

27  
28 284 PC1 separates the images based on the former food type, from the images of sample E to the images  
29  
30  
31 285 of samples A and B. In fact, the former food matrices of sample E have a darker colour, while the  
32  
33 286 former food matrices of samples A and B have a lighter colour.

34  
35 287 The trend observed along PC2 suggests that this principal component differentiates between the  
36  
37 288 images according to the presence of white packaging residues, which are primarily due to paper and  
38  
39  
40 289 plastic. In fact, the images with higher PC2 score values included white packaging residues with  
41  
42 290 higher dimensions.

43  
44 291 As shown in the PC2-PC3 score plot in Figure 5.B, one image of sample F shows a particular  
45  
46 292 behaviour along PC3, with a much higher score than the other images. In fact, this image contains an  
47  
48 293 aluminium residual with a blue spot, which is not present in the other images with aluminium particles.

49  
50  
51 294 Figure 5.C reports the Hotelling  $T^2$  values and Q residuals of the PCA model. The Hotelling  $T^2$  values  
52  
53 295 measure the distance of the samples from the centre of the model (i.e. the origin of the PC space), and  
54  
55  
56 296 therefore describe the variation of each sample within the model. Conversely, the Q residual values  
57  
58 297 indicate how much the description of each sample by the PCA model differs from its actual values.

59  
60



1  
2  
3 298 In other words, samples with high Q residual values show anomalous features, which are not  
4  
5 299 accounted for by the PCA model.  
6  
7  
8 300 Figure 5.C highlights three outlier images: Image 3 has a higher Hotelling  $T^2$  value than the  
9  
10 301 corresponding 99.7% confidence limit, while Image 50 and Image 32 have Q residuals exceeding the  
11  
12 302 99.7% confidence limit.  
13  
14  
15 303 Image 32 has the highest Q residual value, while the corresponding Hotelling  $T^2$  value falls within  
16  
17 304 the 95% confidence limit, thus suggesting that this image has particular features that were not  
18  
19 305 described by the PCA model. In fact, this image shows a red plastic packaging residue, while all the  
20  
21 306 other images with plastic pieces show white or semi-opaque particles.  
22  
23  
24 307 In order to evaluate the colour features with the greatest influence on the Q residual value of Image  
25  
26 308 32, the corresponding contribution plot is shown in Figure 6.A. The colourgram regions with the  
27  
28 309 highest contributions are related to the relative green, hue and PC2 and PC3 score vectors of the PCA  
29  
30 310 models calculated with the various preprocessing methods. As in Figure 4, these colour features can  
31  
32 311 be visualized in the original image domain. For example, considering the rG parameter, the peak in  
33  
34 312 the Q contribution plot falls within the 1341-1358 colourgram interval (highlighted in green in Figure  
35  
36 313 6.A), which corresponds to rG values ranging from 0.24 and 0.30. Figure 6.B reports Image 32 in the  
37  
38 314 original RGB colour domain, while Figure 6.C shows the same sample image in which only the pixels  
39  
40 315 falling in the rG interval previously selected are displayed and the remaining pixels are represented  
41  
42 316 in white. The reconstructed pixels are mainly related to the red plastic piece, confirming that the high  
43  
44 317 Q value of this image is due to the presence of the red packaging residual.  
45  
46  
47  
48  
49  
50

#### 51 319 4. Discussion

52  
53  
54 320 We investigated the potential of RGB imaging coupled with multivariate image analysis strategies  
55  
56 321 for detecting packaging remnants in FFPs. Multivariate image analysis was conducted considering  
57  
58 322 two different approaches: pixel-level analysis and image-level analysis.  
59  
60

1  
2  
3 323 The pixel-level approach (Esbensen et al. 2011; Prats-Montalbán et al. 2011) mainly focused on  
4  
5 324 characterizing the individual pixels in an image and in grouping pixels that share similar features.  
6  
7  
8 325 This approach was tested considering both simple RGB images and augmented RGB images obtained  
9  
10 326 by including additional colour-related parameters in the analysis. The results suggest that including  
11  
12 327 additional colour features in the analysis better highlights the differences that are not clearly visible  
13  
14  
15 328 considering the RGB values alone, in particular when the objects that need to be separated have  
16  
17 329 similar colours.

18  
19 330 The image-level approach simultaneously compares all the images of the dataset, allowing from tens  
20  
21  
22 331 up to hundreds of RGB images to be analysed together (Antonelli et al. 2004; Ulrici et al. 2012;  
23  
24 332 Orlandi et al. 2018a; Orlandi et al. 2018b; Giraudo et al. 2018). The conversion of the RGB images  
25  
26 333 into colourgrams (Antonelli et al., 2004), highlighted both groups of images with similar colour-  
27  
28  
29 334 related features and outlier images, e.g. those containing packaging particles. The PCA model  
30  
31 335 calculated on the colourgram matrix showed that the first source of variability in the image dataset  
32  
33 336 was related to the different colour of the former food matrices from different samples. This suggests  
34  
35 337 that in practical scenarios, the development of specific models for each FFP type may lead to more  
36  
37  
38 338 accurate and reliable results. In this case, it will be necessary to acquire and analyse an adequate  
39  
40 339 number of samples representative of each former food type.

41  
42 340 PCA also highlighted common trends in images with white residues derived from paper or plastic  
43  
44  
45 341 packaging materials and to identify images showing particular features due to the presence of  
46  
47 342 aluminium or differently-coloured plastic remnants.

48  
49 343 Outlier images can be easily detected considering the Hotelling  $T^2$  values and Q residuals, which can  
50  
51 344 be used to build multivariate control charts or classification models capable of automatically detecting  
52  
53  
54 345 images with packaging remnants.

55  
56 346 However, RGB imaging only accounts for colour properties of the imaged samples, which is one  
57  
58 347 limitation of this technique in the detection of packaging materials in FFPs. In fact, in some cases,  
59  
60 348 the packaging residues may be too similar in colour to the FFP particles, making them difficult to

1  
2  
3 349 identify (Tretola et al., 2017a; Tretola et al., 2017b). For example, paperboard is particularly difficult  
4  
5 350 to differentiate from feed material, making its detection complicated and time consuming.  
6  
7  
8 351 In order to overcome this issue, the stereomicroscope could be coupled with more advanced imaging  
9  
10 352 systems capable of detecting light also beyond the visible spectral region, including for example the  
11  
12 353 near infrared spectral region (Gowen et al., 2011; Ferrari et al., 2013; Dale et al., 2013; Ulrici et al.,  
13  
14 354 2013; Amigo et al., 2015; Calvini et al., 2016; Vermeulen et al., 2017; Calvini et al., 2018). The  
15  
16  
17 355 colour features of the samples derived from RGB images could be combined with spectral features  
18  
19 356 derived from multispectral or hyperspectral images, thus leading to a more comprehensive  
20  
21  
22 357 characterization of the differences between former food matrices and residues of packaging materials.  
23  
24 358

## 26 359 5. Conclusions

28 360 **The present work is a preliminary study focused on the potential of imaging methods applied to feed**  
29  
30  
31 361 **and food safety.** Identifying packaging remnants in former food products is important in ensuring the  
32  
33 362 safety of FFPs used as feed ingredients. Generally, control procedures for the determination of  
34  
35 363 packaging residues in feed are based on the visual inspection and manual selection of undesirable  
36  
37  
38 364 contaminant materials.

40 365 To overcome the drawbacks of these procedures, **we have explored the feasibility of using** RGB  
41  
42 366 imaging as a rapid and non-destructive tool for the automated detection of packaging particles in FFPs.  
43  
44  
45 367 In this paper, we have assessed the various features of this technique, together with the challenges  
46  
47 368 related to the application of image analysis strategies.

49 369 **The preliminary results obtained in this study demonstrate the potential** of the proposed approach, in  
50  
51 370 particular when the colour of the undesirable packaging residues can be differentiated from the colour  
52  
53  
54 371 of the ex-food matrix.

56 372 In order to develop more robust and sensitive models, we plan to increase the size of the image dataset  
57  
58 373 by acquiring a higher number of images representative of each FFP type.  
59  
60

374

## 6. Acknowledgements

The present work has been done in the frame of the following projects: Sustainable feed design applying circular economy principles: the case former food in pig nutrition (SUSFEED) funded by the Fondazione Cariplo, call "Economia circolare: ricerca per un futuro sostenibile"; Progetto di Grande Rilavenza IT-RS "Sustainable animal nutrition" (SUN) funded the Ministero degli Affari Esteri e della Cooperazione Internazionale.

## 7. Declaration of interest statement

The authors declare that they have no conflict of interest.

For Peer Review Only

1  
2  
3  
4  
5  
6  
7  
8  
9  
10  
11  
12  
13  
14  
15  
16  
17  
18  
19  
20  
21  
22  
23  
24  
25  
26  
27  
28  
29  
30  
31  
32  
33  
34  
35  
36  
37  
38  
39  
40  
41  
42  
43  
44  
45  
46  
47  
48  
49  
50  
51  
52  
53  
54  
55  
56  
57  
58  
59  
60**References**

- Amato G, Desiato R, Giovannini T, Pinotti L, Tretola M, Gili M, Marchis D. 2017. Gravimetric quantitative determination of packaging residues in feed from former food. *Food Addit Contam Part A*. 34(8), 1446-1450. doi: 10.1080/19440049.2017.1337277
- Amigo JM, Babamoradi H, Elcoroaristizabal S. 2015. Hyperspectral image analysis. A tutorial. *Analytica Chimica Acta*. 896, 34-51. doi: 10.1016/j.aca.2015.09.030
- Antonelli A, Cocchi M, Fava P, Foca G, Franchini GC, Manzini D, Ulrici A. 2004. Automated evaluation of food colour by means of multivariate image analysis coupled to a wavelet-based classification algorithm. *Analytica Chimica Acta*. 515(1), 3-13. doi: 10.1016/j.aca.2004.01.005
- Calvini R, Foca G, Ulrici A. 2016. Data dimensionality reduction and data fusion for fast characterization of green coffee samples using hyperspectral sensors. *ABC*. 408(26), 7351-7366. doi: 10.1007/s00216-016-9713-7
- Calvini R, Orlandi G, Foca G, Ulrici A. 2018. Development of a classification algorithm for efficient handling of multiple classes in sorting systems based on hyperspectral imaging. *JSI*. 7, a13. doi: 10.1255/jsi.2018.a13
- Calvini R, Orlandi G, Foga G, Ulrici A. 2020. Colourgrams GUI: A graphical user-friendly interface for the analysis of large datasets of RGB images. *Chemom. Intell. Lab. Syst.* 196(15), 103915. doi: 10.1016/j.chemolab.2019.103915
- Cheli F, Bontempo V, Pinotti L, Ottoboni M, Tretola M, Baldi A, Dell'Orto V. 2018. Feed Analysis and Animal Nutrition: Electronic Nose as a Diagnostic Tool. *Chem Eng Trans*. 68, 223-228.
- Dale LM, Thewis A, Boudry C, Rotar I, Dardenne P, Baeten V, Pierna JAF. 2013. Hyperspectral imaging applications in agriculture and agro-food product quality and safety control: A review. *Appl Spectrosc Rev*. 48(2), 142-159. doi: 10.1080/05704928.2012.705800
- Dorrepaal R, Malegori C, Gowen A. 2016. Tutorial: Time series hyperspectral image analysis. *J Near Infrared Spec*. 24(2), 89-107. doi: 10.1255/jnirs.1208
- Duchesne C, Liu JJ, MacGregor JF. 2012. Multivariate image analysis in the process industries: A review. *Chemom Intell Lab Syst*. 117, 116-128. doi: 10.1016/j.chemolab.2012.04.003
- Esbensen K, Geladi P. 1989. Strategy of multivariate image analysis (MIA). *Chemom Intell Lab Syst*. 7(1-2), 67-86. doi: 10.1016/0169-7439(89)80112-1
- Ferrari C, Foca G, Ulrici A. 2013. Handling large datasets of hyperspectral images: Reducing data size without loss of useful information. *Analytica Chimica Acta*. 802, 29-39. doi: 10.1016/j.aca.2013.10.009
- Geladi P, Isaksson H, Lindqvist L, Wold S, Esbensen K. 1989. Principal component analysis of multivariate images. *Chemom Intell Lab Syst*. 5(3), 209-220. doi: 10.1016/0169-7439(89)80049-8
- Giraud A, Calvini R, Orlandi G, Ulrici A, Geobaldo F, Savorani F. 2018. Development of an automated method for the identification of defective hazelnuts based on RGB image analysis and colourgrams. *Food Control*. 94, 233-240. doi: 10.1016/j.foodcont.2018.07.018

1

2

3 422 Giromini C, Ottoboni M, Tretola M, Marchis D, Gottardo D, Caprarulo V, Baldi A, Pinotti L. 2017.  
4 423 Nutritional evaluation of former food products (ex-food) intended for pig nutrition. *Food Add Contam*  
5 424 *Part A.* 34(8),1436-1445.

7 425 Gowen AA, Marini F, Esquerre C, O'donnell C, Downey G, Burger J. 2011. Time series  
8 426 hyperspectral chemical imaging data: challenges, solutions and applications. *Analytica Chimica Acta.*  
9 427 705(1-2), 272-282. doi: 10.1016/j.aca.2011.06.031

11 428 Kucheryavskiy S. 2013. A new approach for discrimination of objects on hyperspectral images.  
12 429 *Chemom Intell Lab Syst.* 2013 120, 126-135. doi: 10.1016/j.chemolab.2012.11.009

15 430 Orlandi G, Calvini R, Foca G, Ulrici A. 2018a. Automated quantification of defective maize kernels  
16 431 by means of Multivariate Image Analysis. *Food Control.* 85, 259-268. doi:  
17 432 10.1016/j.foodcont.2017.10.008

19 433 Orlandi G, Calvini R, Pigani L, Foca G, Simone, G. V., Antonelli, A., Ulrici, A. 2018b. Electronic  
20 434 eye for the prediction of parameters related to grape ripening. *Talanta.* 186, 381-388. doi:  
21 435 10.1016/j.talanta.2018.04.076

24 436 Ottoboni M, Tretola M, Luciano A, Giuberti G, Gallo A, Pinotti L. 2019. Carbohydrate digestion and  
25 437 predicted glycemic index of bakery/confectionary ex-food intended for pig nutrition. *Italian Journal*  
26 438 *of Animal Science.* 1, 838–849. doi: 10.1080/1828051X.2019.1596758

28 439 Pinotti L, Giromini C, Ottoboni M, Tretola M, Marchis D. 2019. Review: insects and former  
30 440 foodstuffs for upgrading food waste biomasses/streams to feed ingredients for farm animals. *Animal.*  
31 441 1-11. doi: 10.1017/S1751731118003622

33 442 Prats-Montalbán, J. M., De Juan, A., Ferrer, A. 2011. Multivariate image analysis: a review with  
34 443 applications. *Chemometrics and Intelligent Laboratory Systems.* 107(1), 1-23. doi:  
35 444 10.1016/j.chemolab.2011.03.002

37 445 Tretola M, Di Rosa A, Tirloni E, Ottoboni M, Giromini C, Leone F, Bernardi CEM, Dell'Orto V,  
38 446 Chiofalo V, Pinotti L. 2017a. Former food products safety: microbiological quality and computer  
39 447 vision evaluation of packaging remnants contamination. *Food Addit Contam Part A.* 34(8), 1427-  
40 448 1435. doi: 10.1080/19440049.2017.1325012

43 449 Tretola M, Ottoboni M, Di Rosa A, Giromini C, Fusi E, Rebucci R, Leone F, Dell'Orto V, Chiofalo  
44 450 V, Pinotti L. 2017 b. Former Food Products Safety Evaluation: Computer Vision as an Innovative  
45 451 Approach for the Packaging Remnants Detection. *J Food Qual.* 1-6. doi: 10.1155/2017/1064580

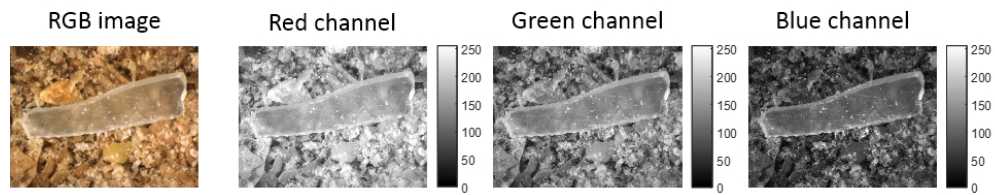
47 452 Tretola M, Ottoboni M, Luciano A, Dell'Orto V, Cheli F, Pinotti L. 2019a. Tracing food packaging  
48 453 contamination: an electronic nose applied to leftover food. *Food Addit Contam Part A.* 36, 1748-1756.  
49 454 doi: 10.1080/19440049.2019.1653498

51 455 Tretola M, Ottoboni M, Luciano A, Rossi L, Baldi A, Pinotti L. 2019b. Former food products have  
52 456 no detrimental effects on diet digestibility, growth performance and selected plasma variables in post-  
53 457 weaning piglets. *IJAS.* 18, 987-996. doi.org/10.1080/1828051X.2019.1607784

56 458 Tretola M, Luciano A, Ottoboni M, Baldi A, Pinotti L. 2019c. Influence of Traditional vs Alternative  
57 459 Dietary Carbohydrates Sources on the Large Intestinal Microbiota in Post-Weaning Piglets. *Animals.*  
58 460 9(8), 516. <https://doi.org/10.3390/ani9080516>.

60 461

- 1  
2  
3 462 Ulrici A, Foca G, Ielo MC, Volpelli LA, Lo Fiego DP. 2012. Automated identification and  
4 463 visualization of food defects using RGB imaging: Application to the detection of red skin defect of  
5 464 raw hams. *Innov Food Sci Emerg Tech.* 16, 417-426. doi: 10.1016/j.ifset.2012.09.008  
6  
7  
8 465 Ulrici A, Serranti S, Ferrari C, Cesare D, Foca G, Bonifazi G. 2013. Efficient chemometric strategies  
9 466 for PET–PLA discrimination in recycling plants using hyperspectral imaging. *Chemom Intel Lab Syst.*  
10 467 122, 31-39. doi: 10.1016/j.chemolab.2013.01.001  
11  
12 468 van Raamsdonk LWD, Pinckaers VGZ., Vliege JJM, van Egmond HJ. 2012. Examination of  
13 469 packaging materials in bakery products: a validated method for detection and quantification. RIKILT  
14 470 Report - Wageningen, the Netherlands. 1–20.  
15  
16 471 van Raamsdonk LWD, Rijk R, Schouten GPJ, Mennes W, Meijer GAL, Poel AFBVD, De Jong J.  
17 472 2011. A risk evaluation of traces of packaging materials in former food products intended as feed  
18 473 materials. RIKILT Report - Wageningen, the Netherlands. 1–69.  
19  
20  
21 474 **van Raamsdonk LWD, van der Zande M, Koelmans AA, Hoogenboom RL, Peters RJ, Groot MJ,**  
22 475 **Peijnenburg Ad ACM, Weesepeel, Y. J. 2020. Current Insights into Monitoring, Bioaccumulation,**  
23 476 **and Potential Health Effects of Microplastics Present in the Food Chain. *Foods*, 9(1), 1-28.**  
24 477 **doi:10.3390/foods9010072**  
25  
26 478 Vermeulen P, Ebene MB, Orlando B, Fernández Pierna JA, Baeten V. 2017. Online detection and  
27 479 quantification of particles of ergot bodies in cereal flour using near-infrared hyperspectral imaging.  
28 480 *Food Add Contam Part A.* 34(8), 1312-1319. doi: 10.1080/19440049.2017.1336798  
29  
30  
31 481  
32  
33 482  
34  
35  
36  
37  
38  
39  
40  
41  
42  
43  
44  
45  
46  
47  
48  
49  
50  
51  
52  
53  
54  
55  
56  
57  
58  
59  
60



16 Figure 1. RGB image of a sample contaminated with a plastic residue and gray-scale images of the  
17 corresponding red, green and blue channels.

18  
19 256x71mm (96 x 96 DPI)



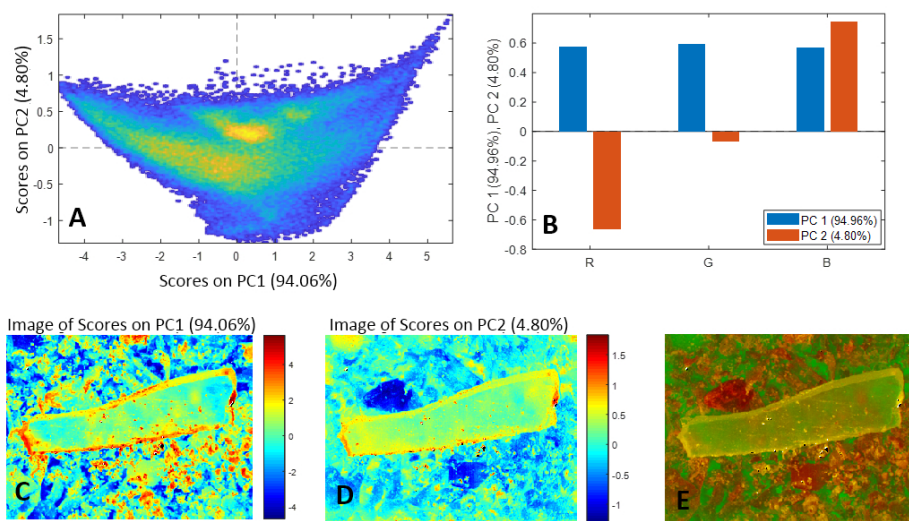


Figure 2. Results of the PCA model calculated on the RGB image of a former food sample with a plastic residue. In A: PC1 - PC2 score plot; in B: PC1 - PC2 loading plot; in C: PC1 score image; in D: PC2 score image and in E: false-colour PC1-PC2 score image.

295x166mm (96 x 96 DPI)

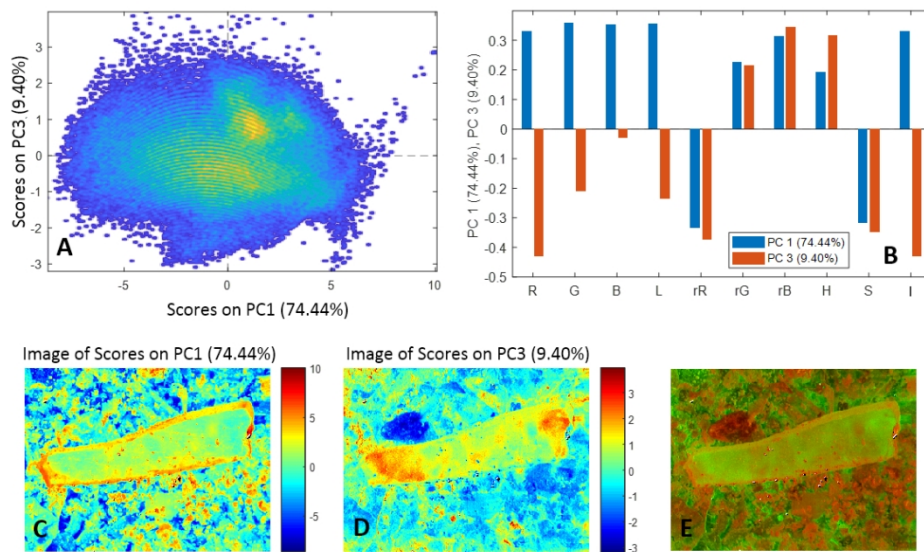


Figure 3. Results of the PCA model calculated on the augmented RGB image of a former food sample with a plastic residue. In A: PC1 – PC3 score plot; in B: PC1 – PC3 loading plot; in C: PC1 score image; in D: PC3 score image and in E: false-colour PC1-PC3 score image.

317x189mm (96 x 96 DPI)

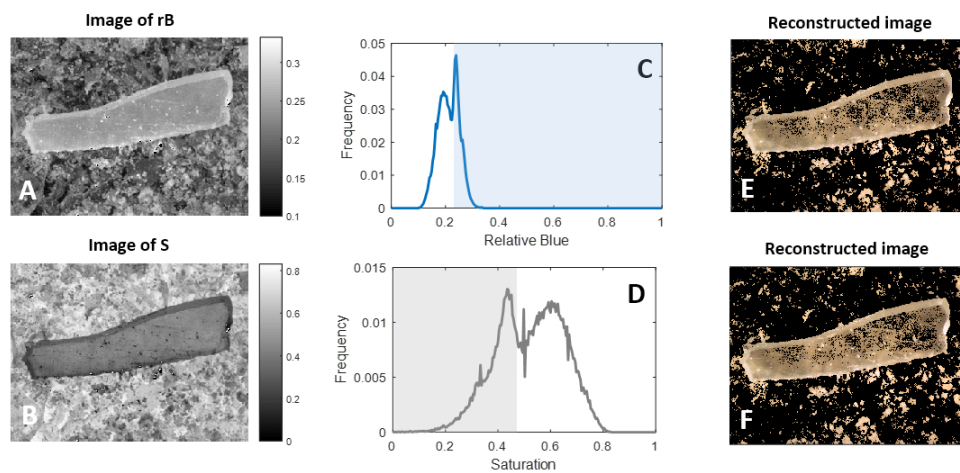
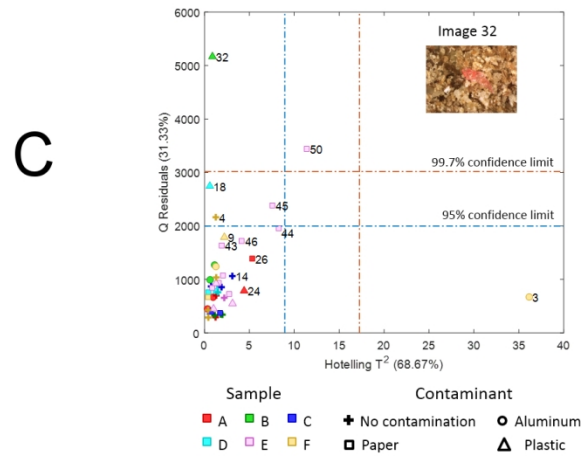
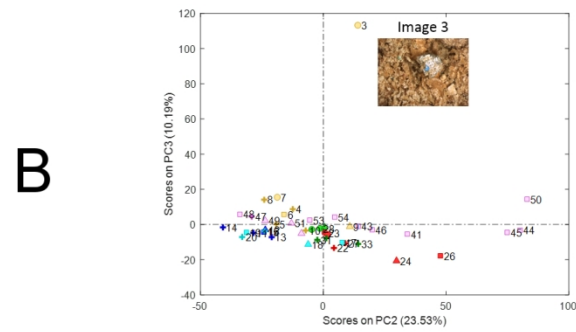
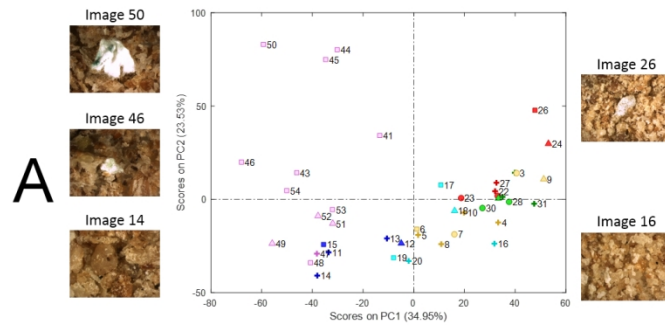


Figure 4. Gray-scale images of relative blue (A) and saturation (B); frequency distribution curves of relative blue (C) and saturation (D); images reconstructed using the selected features of relative blue (E) and saturation (F).

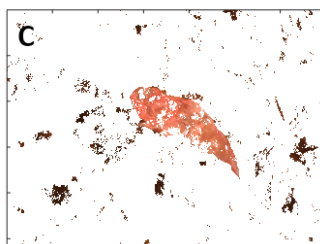
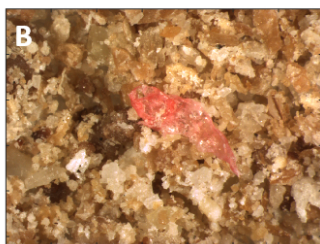
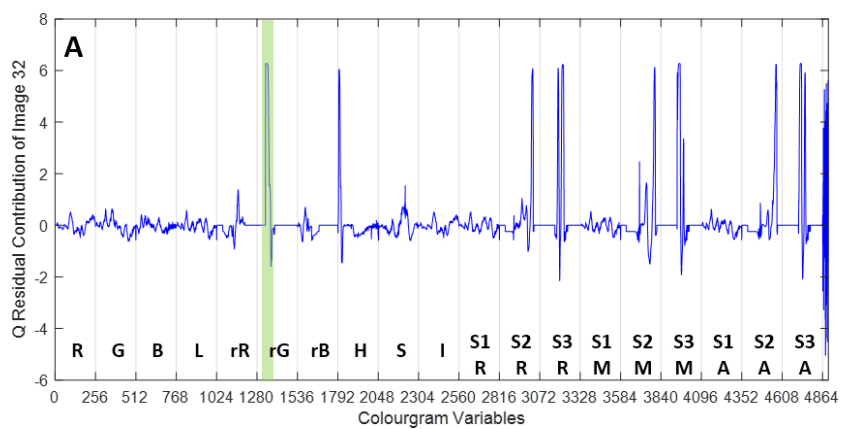
293x150mm (96 x 96 DPI)



45 Results of the PCA model calculated on the colourgrams matrix. In A: PC1-PC2 score plot; in B: PC2-PC3  
46 score plot; in C: Hotelling T2 and Q residuals plot.

47 89x159mm (300 x 300 DPI)

1  
2  
3  
4  
5  
6  
7  
8  
9  
10  
11  
12  
13  
14  
15  
16  
17  
18  
19  
20  
21  
22  
23  
24  
25  
26  
27  
28  
29  
30  
31  
32  
33  
34  
35  
36  
37  
38  
39  
40  
41  
42  
43  
44  
45  
46  
47  
48  
49  
50  
51  
52  
53  
54  
55  
56  
57  
58  
59  
60



Q residual contribution plot of Image 32 (A), original Image 32(B), and Image 32 reconstructed using the selected features (C).

87x62mm (300 x 300 DPI)

**Table 1.** Summary of the FFP samples considered in this study and corresponding number of acquired images.

Sample name	Total n° of images	Main food product types	Images with no residues	Images with plastic residues	Images with paper residues	Images with aluminum residues
<b>A</b>	6	confectionery products	2	1	1	2
<b>B</b>	6	confectionery products	3	1	0	2
<b>C</b>	5	confectionery products	3	1	1	0
<b>D</b>	5	baked goods and confectionery products	2	1	2	0
<b>E</b>	13	confectionery products	1	3	9	0
<b>F</b>	8	baking industry	4	1	1	2
<b>Total</b>	<b>43</b>		<b>15</b>	<b>8</b>	<b>14</b>	<b>6</b>

1  
2  
3  
4  
5  
6  
7  
8  
9  
10  
11  
12  
13  
14  
15  
16  
17  
18  
19  
20  
21  
22  
23  
24  
25  
26  
27  
28  
29  
30  
31  
32  
33  
34  
35  
36  
37  
38  
39  
40  
41  
42  
43  
44  
45  
46  
47  
48  
49  
50  
51  
52  
53  
54  
55  
56  
57  
58  
59  
60**Table 2.** Colour-related parameters used to calculate the augmented RGB image.

Name	Abbreviation	Equation
Lightness	L	$L = R + G + B$
Relative Red	rR	$rR = R / L$
Relative Green	rG	$rG = G / L$
Relative Blue	rB	$rB = B / L$
Hue	H	Value ranging from 0 to 1, corresponding to a colour transition from red to orange, yellow, green, cyan, blue, magenta, and finally back to red.
Saturation	S	$S = [\max(R, G, B) - \min(R, G, B)] / \max(R, G, B)$
Intensity	I	$I = \max(R, G, B)$